[19]W. E. Baylis, J. Chem. Phys. 51, 2665 (1969).
[20]Stogryn and Hirschfelder found similar results for Ar_2 molecules: Except at quite low temperatures and pressures, where collision rates are low, most quasi-bound resonances may be treated as bound states. See Ref. 4.

PHYSICAL REVIEW A VOLUME 1, NUMBER 4 APRIL 1970

Hyperfine Structure of Sodium†

T. Lee, N. C. Dutta, and T. P. Das
Department of Physics, University of California, Riverside, California 92502*
(Received 15 August 1969)

The Brueckner-Goldstone many-body perturbation theory has been applied in a calculation of hyperfine structure (hfs) of sodium in the ground ($^2S_{1/2}$) state. Our result for A (as in $A\vec{I}\cdot\vec{J}$) is 857.8001 ± 6 Mc/sec, in good agreement with the experimental result of 885.8131 ± 0.0001 Mc/sec. The major contributions beyond the restricted Hartree-Fock result of 622.6430 Mc/sec arise from diagrams describing the exchange core-polarization effect. This contributes 139.6665 Mc/sec, in agreement with the existing unrestricted Hartree-Fock (UHF) and moment-perturbation (MP) results. All diagrams involving two orders of correlation interactions and associated ladders were calculated and were found to contribute 95.49 Mc/sec. Higher-order diagrams involving three or more orders of correlation interaction were investigated and found to be of minor importance in affecting the hfs constant of soidum.

I. INTRODUCTION

The Brueckner-Goldstone (BG) many-body linked-cluster perturbation theory[1,2] has been applied successfully[3–9] in the past to the study of hyperfine properties of a number of atomic systems. This method is especially suitable for the hyperfine-structure (hfs) problem for three main reasons. First, it allows various types of correlation effects, which are usually neglected in conventional one-electron theory, to be treated systematically by a perturbation procedure utilizing a suitably chosen orthonormal basis set. Secondly, the use of diagrammatic techniques in this method enables one to gain considerable physical insight and assess the relative importance of the contributions to hfs from different physical processes, such as exchange core-polarization (ECP), inter- and intra-shell correlations, self-consistency, and mutual polarization of orbitals. Thirdly, being a perturbation theory, it handles small quantities rather than the differences of large up- and down-spin densities as in the unrestricted Hartree-Fock (UHF) theory.[10] The most remarkable example where these techniques have been demonstrated to be particularly successful is the phosphorus atom,[7] where the BG many-body procedure has not only provided good agreement in magnitude with experiment but has also removed the discrepancy in sign that was found with the UHF theory.[11]

The purpose of the present paper is to report the results of our calculation on the hfs constant A (in the spin-Hamiltonian term $A\vec{I}\cdot\vec{J}$) for atomic sodium in its ground state (^2S). Accurate experimental data are available for A in this atom,[12] but no calculations for A incorporating many-body effects are available in the literature. However, one-electron calculations are available for the direct and core-polarization effects in this atom, the latter through UHF as well as perturbation procedures[13,14] based on a differential equation approach. It is interesting to inquire into how these results compare with those from the one-electron BG diagrams and the nature of many-body effects as well as the comparison with experiment of the total result by the BG procedure.

In Sec. II, we present very briefly the pertinent features of BG theory as applied here to hfs calculations. Section III involves a description of all the important diagrams and our results for the sodium atom. Section IV contains the discussion and comparison of our results with earlier one-electron results and experiments.

II. THEORY

A. Resume of BG Theory

The total nonrelativistic Hamiltonian for an atomic system of N electrons is

$$\mathcal{H} = \sum_{i=1}^{N} T_i + \sum_{i<j} v_{ij} \quad , \tag{1}$$

where T_i represents the sum of the kinetic energy

and nuclear Coulomb potential of the ith electron, and v_{ij} is the electrostatic interaction potential between electrons i and j. For the study of atomic properties, one is interested in the exact solution of the Schrödinger equation

$$\mathcal{H}\Psi_0 = E\Psi_0 \quad . \tag{2}$$

In the perturbation procedure used here one replaces the Hamiltonian $\mathcal{H}$ by a one-electron Hamiltonian,

$$\mathcal{H}_0 = \sum_{i=1}^{N} (T_i + V_i) \quad , \tag{3}$$

and treats $\mathcal{H}' = \mathcal{H} - \mathcal{H}_0$ as a small perturbation. The single-particle potential V_i is selected in such a way that the one-electron equation

$$(T + V)\varphi_i = \epsilon_i \varphi_i \tag{4}$$

can be conveniently solved for a complete set of states with eigenvalues ϵ_i including the continuum. A normalized zero-order determinantal wave function Φ_0 can be formed out of N of these single particle states which satisfy the unperturbed Schrödinger equation

$$\mathcal{H}_0\Phi_0 = E_0\Phi_0 \quad . \tag{5}$$

The normalized eigenfunction Ψ_0 of the total Hamiltonian $\mathcal{H}$ could be generated from the unperturbed eigenfunction Φ_0 of $\mathcal{H}_0$ by slowly "turning on" the perturbation "adiabatically" and using the unitary time-development operator[15] U defined by

$$\Psi_0 = U(0, -\infty)\Phi_0 \quad . \tag{6}$$

Using this normalized eigenfunction Ψ_0, the expectation value of an operator O is given by

$$\langle O \rangle = \langle \Psi_0 | O | \Psi_0 \rangle \quad .$$

Making use of Eq. (6), one can use procedures available in the literature to show that only linked diagrams occur in the expectation value.[1] The essential steps are

$$\begin{aligned}
\langle O \rangle &= \langle U(0, -\infty)\Phi_0 | O | U(0, -\infty)\Phi_0 \rangle \\
&= \langle U(0, \infty) U(\infty, -\infty)\Phi_0 | O | U(0, -\infty)\Phi_0 \rangle \\
&= \langle U(\infty, -\infty)\Phi_0 | U(\infty, 0) O U(0, -\infty) | \Phi_0 \rangle \\
&= \frac{\langle \Phi_0 | U(\infty, 0) O U(0, -\infty) | \Phi_0 \rangle}{\langle \Phi_0 | U(\infty, -\infty) | \Phi_0 \rangle} \\
&= \langle \Phi_0 | U(\infty, 0) O U(0, -\infty) | \Phi_0 \rangle_L \quad ,
\end{aligned} \tag{7}$$

where L indicates that the summation is over linked terms only, and the last but one stop follows from considerations of adiabatic switching; namely,

$$U(\infty, -\infty)\Phi_0 = e^{i\eta}\Phi_0 .$$

The time-development operator $U(t, t_0)$ is expanded in the usual perturbation series

$$U(t, t_0) = 1 + \sum_{n=1}^{\infty} U_n(t, t_0) \quad ,$$

where $U_n(t, t_0) = (-i)^n \int_{t_0}^{t} dt_1$

$$\times \int_{t_0}^{t_1} dt_2 \cdots \int_{t_0}^{t_{n-1}} dt_n \mathcal{H}_I'(t_1)\mathcal{H}_I'(t_2)\cdots\mathcal{H}_I'(t_n) \, . \tag{8}$$

The suffix I refers to the interaction representation.

In the past,[3,4,6-8] a different normalization procedure has been utilized; namely, $\langle \Phi_0 | \Psi_0 \rangle = 1$, so that $\langle \Psi_0 | \Psi_0 \rangle \neq 1$; one now has a linked-cluster expansion for the wave function

$$\Psi_0 = \sum_{n=1}^{\infty} {}^{L} U_n(0, -\infty)\Phi_0 \quad .$$

The expectation value is then given by

$$\langle O \rangle = \langle \Psi_0 | O | \Psi_0 \rangle / \langle \Psi_0 | \Psi_0 \rangle \quad .$$

The numerator of this expression has some unlinked terms in it. However, an expansion of the denominator shows that it cancels the above-mentioned unlinked terms, showing that both procedures are in principle equivalent. In the present calculation, we have utilized Eq. (7). For purposes of actual calculation of diagrams one carries out the time integrations in Eq. (8) and rewrites Eq. (7) in the form

$$\begin{aligned}
\langle O \rangle = \sum_n \sum_m \langle \Phi_0 | [\mathcal{H}'(E_0 - H_0)^{-1}]^n \\
\times O[(E_0 - H_0)^{-1}\mathcal{H}']^m | \Phi_0 \rangle_L \quad .
\end{aligned} \tag{9}$$

Each term of Eq. (9) can be represented by a group of Feynman-like diagrams drawn according to rules enumerated elsewhere.[2-9] Similar terminology has been utilized as in earlier work with corresponding notations for vertices associated with the interactions v_{ij} and V_i. Particle and hole states are represented as solid lines directed, respec-

tively, upward and downward with the time axis being directed upwards.

B. Basis Set

For the single-particle potential V, we have chosen the V^{N-1} potential.[2-8] This potential generates a complete set of orthonormal states which include an infinite number of bound states in addition to the continuum states. The continuum states were normalized by a procedure outlined elsewhere.[6,16] The bound states ($\epsilon_i < 0$) are characterized by the quantum numbers n, l, and m, as in

$$\varphi_i = [P(nl;r)/r]\, Y_l^m(\theta,\phi)\,\chi_\sigma(m_\sigma) \quad .$$

The continuum states ($\epsilon_i = k^2/2$) are formally similar, with the principal quantum number n replaced by the continuously varying parameter k. The s states ($l=0$) are generated in the field of a neutral sodium atom minus the $3s$ electron. All the $l \neq 0$ states are calculated in the field of a neutral sodium atom minus one $2p$ electron, an average being taken over the three possible m_l values ($\pm 1, 0$) for this electron.[6,7] The corresponding radial equations are as follows:

$l=0$ states

$$\left(\frac{d^2}{dr^2} + \frac{2N}{r} - \frac{1}{r}[4Y_0(1s^0,1s^0;r) + 4Y_0(2s^0,2s^0;r) + 12Y_0(2p^0,2p^0;r)] + 2\epsilon_{ns}\right)P(ns;r)$$

$$+ \frac{2}{r}\left(P(1s^0;r)Y_0(1s^0,ns;r) + P(2s^0;r)Y_0(2s^0,ns;r) + P(2p^0;r)Y_1(2p^0,ns;r)\right) = 0 \quad . \tag{10}$$

The matrix element for this potential is shown schematically in Fig. 1.

$l \neq 0$ states

$$\left[\frac{d^2}{dr^2} + \frac{2N}{r} - \frac{l(l+1)}{r^2} - \frac{1}{r}\left(4Y_0(1s^0,1s^0;r) + 4Y_0(2s^0,2s^0;r) + 2Y_0(3s^0,3s^0;r)\right.\right.$$

$$\left.\left. + 10Y_0(2p^0,2p^0;r) - \frac{4}{25[4l(l+1)-3]}\,Y_2(2p^0,2p^0;r)\right) + 2\epsilon_{nl}\right]P(nl;r)$$

$$+ \frac{1}{(2l+1)r}\left(2P(1s^0;r)Y_l(1s^0,nl;r) + 2P(2s^0,r)Y_l(2s^0,nl;r) + P(3s^0;r)Y_l(3s^0,nl;r)\right.$$

$$\left. + \frac{8l(l-1)}{(2l-1)^2}P(2p^0;r)Y_{l-1}(2p^0,nl;r) + \frac{8(l+1)(l+2)}{(2l+3)^2}P(2p^0;r)Y_{l+1}(2p^0,nl;r)\right) = 0 \quad , \tag{11}$$

where $Y_k(nl,n'l';r) = r\int_0^\infty \frac{r_<^k}{r_>^{k+1}} P(nl;r')\,P(n'l';r')\,dr'$.

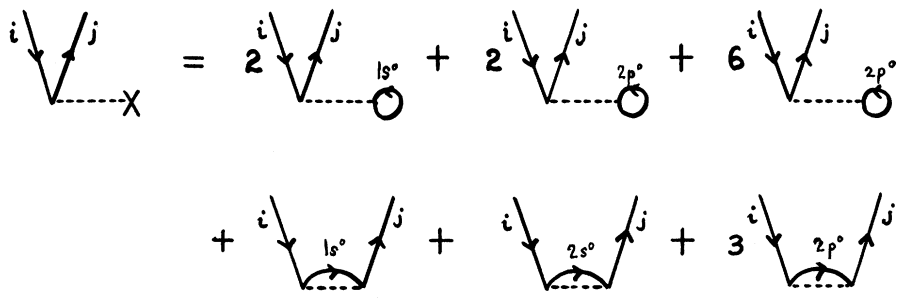

FIG. 1. Diagrammatic representation of the single-particle potential V^{N-1} for the s state.

In Eqs. (10) and (11) and in subsequent equations, the superscript zero is used to denote that the Hartree-Fock wave functions are used. For the core states, we have wave functions from Clementi's table.[17] The $3s$ and $2p$ basis functions that we obtained from Eqs. (10) and (11) were almost identical (up to the third decimal figure) with the $3s^0$ and $2p^0$ input wave functions, as also were the one-electron energies ϵ_{3s0} and ϵ_{2p0} as compared to ϵ_{3s} and ϵ_{2p} (up to the fourth decimal figure). The one-electron energies ϵ_{1s} and ϵ_{2s} as expected[2,6,7] differed more markedly from ϵ_{1s0} and ϵ_{2s0}, these differences being carefully accounted for in our calculations through "ladder" diagrams.[2-9] The differences between P_{1s} and P_{1s0} and P_{2s} and P_{2s0}, while more significant than in the case of the $3s$ and $2p$ states, were not substantial enough to influence the expectation values of the relevant operators that occur in the diagrams and were neglected.

C. Expectation Value of the hfs Operator

Only the Fermi contact interaction[18] contributes to the magnetic hfs of the ground state of sodium because it has only a single unpaired $3s$ electron. The perturbation Hamiltonian corresponding to the contact interaction is given by[18]

$$\mathcal{H}_{\rm hfs}=\frac{16\pi}{3}\frac{\mu_B\mu_N}{Ia_B^3}\vec{I}\cdot\sum_{i=1}^{N}\vec{S}_i\delta(\vec{r}_i), \tag{12}$$

with $\vec{I}$ and $\vec{S}_i$ being the nuclear and electron spin operators, a_B the Bohr radius, and μ_B and μ_N representing the Bohr magneton and nuclear magnetic moment, respectively. In an experimental determination of the hyperfine structure, one is interested in the hfs constant A, defined in the present case by the spin Hamiltonian,

$$\mathcal{H}_{\rm spin}=A\vec{I}\cdot\vec{S}\quad .$$

Using Eq. (12), A is given by

$$A=\frac{16\pi}{3}\frac{\mu_B\mu_N}{ISa_B^3}\left\langle\Psi_0\left|\sum_{i=1}^{N}S_{zi}\delta(\vec{r}_i)\right|\Psi_0\right\rangle\ , \tag{13}$$

where Ψ_0 refers to the state with magnetic quantum number $M_S=S$. Equation (13) may be expanded in a perturbation series using Eq. (9),

$$A=\frac{16\pi\mu_B\mu_N}{3ISa_B^3}\sum_{n,m}\left\langle\Phi_0\left|\left(\mathcal{H}'\frac{1}{E_0-\mathcal{H}_0}\right)^n\right.\right.$$

$$\times\sum S_{zi}\delta(\vec{r}_i)\left(\frac{1}{E_0-\mathcal{H}_0}\mathcal{H}'\right)^m\left|\Phi_0\right\rangle_L\ , \tag{14}$$

where the term associated with $U_n(\infty,0)$ and $U_m(0,-\infty)$ is referred to as the (m,n) term and the corresponding diagram as (m,n) diagram. On account of the Hermiticity of the operators involved in Eq. (14), the contributions from (m,n) and (n,m) diagrams are equal. In the past,[3,6,8] three different choices have been used for the vertex and operator associated with the hyperfine interaction. The specific choice is of course unimportant in the final result because the conversion factor from the diagram to A is adjusted accordingly. For the sake of uniformity, we shall adopt the notation in a recent paper on the lithium atom ^2P state, the hfs vertex diagram being associated with $2s_z\delta(\vec{r})$. The corresponding conversion factor for expressing A in megacycles is given by

$$C=(8\pi/3)(\mu_B\mu_N/ISa_B^3h)\times10^{-6}\quad .$$

Using[19] $\mu_B=9.2731\times10^{-21}$ erg G^{-1}, $\mu_N(\mathrm{Na}^{23})=2.21753\times0.505038\times10^{-23}$ erg G^{-1}, $a_B=0.529172\times10^{-8}$ cm, and $h=6.62517\times10^{-27}$ erg/sec., we get $C=1181.65$ Mc/sec.

III. DIAGRAMS AND RESULTS

In this section, we present the results of our calculation. In Fig. 2, we show the (0,0), (0,1), and some important (1,1) diagrams. The (0,0) diagram

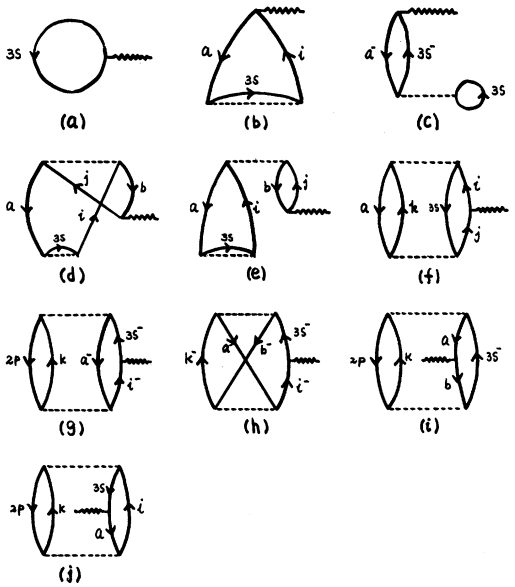

FIG. 2. (a) represents (0,0) diagram; (b) and (c) (0,1) diagrams; and (d)–(j) some of the (1,1) diagrams. In these diagrams, states a and b denote hole states ($1s$, $2s$, and $2p$), whereas i, j, and k symbolize the particle states.

shown in Fig. 2(a) represents the direct contribution from the $3s$ electron in the restricted Hartree-Fock (RHF) approximation. It contributes 622.6436 Mc/sec to the hfs constant which is 70% of the experimental value. One expects the remainder to arise mainly from the unsymmetric interaction between the spin-up valence electron and the spin-up and spin-down core electrons. This unsymmetric interaction is composed of exchange core-polarization and various correlation and polarization effects. Besides this, one expects some contribution from the additional phase space for excitation of core electrons in spin-down states, since the $3s^-$ state[20] is empty while the $3s^+$ is occupied. The diagram associated with the latter effect will be referred to as phase space or residue diagrams. These observations manifest themselves in the hfs diagrams through the fact that at least one $3s^+$ hole line or one $3s^-$ particle line occurs in all the diagrams.

Thus, considering first the (0, 1) diagrams, Fig. 2(b) describes the exchange polarization of the core s-electrons by the $3s$ electron, while 2(c) is a residue diagram. The spin density arising from diagram 2(b) is given by the expression

$$\sum_{ks} \frac{\langle 3sks|v|ns3s\rangle\langle ns|2\delta(\vec{r})s_z|ks\rangle}{\epsilon_{ns}-\epsilon_{ks}}\,;\ ns=1s,2s, \tag{15}$$

where the summation has the usual meaning of a regular summation over the bound states and an integration over the continuum states. As a consequence of the use of the V^{N-1} potential for generating the s states, ladder corrections have to be applied to the ECP diagrams. For s states, these corrections come about in the following way. The difference between the Hartree-Fock potential and the V^{N-1} potential can be written for an electron in an s state j as

$$\sum_m \left(\langle jm|v|jm\rangle - \langle jm|v|mj\rangle\right) - \sum_{m^0\neq 3s^0} \left(\langle jm^0|v|jm^0\rangle - \langle jm^0|v|m^0j\rangle\right) \quad , \tag{16}$$

where the summation is over the hole states. If we ignore the difference between the wave functions for m and m^0 states, a justifiable approximation, the correction in (16) vanishes for $j=3s$, and for other hole s states it reduces to the form

$$\langle j3s|v|j3s\rangle - \langle j3s|v|3sj\rangle \quad . \tag{17}$$

The insertion of this correction vertex on the hole lines in individual diagrams and summation to all orders, described as the hole-hole ladder effect, results in a shift of the energy denominators ocurring in the diagrams by the amount in (17).[2-9]

Thus, in sodium the hole-hole ladder correction to the energy denominator corresponds to the difference between the Hartree-Fock energies for the $j(j=1s, 2s)$ states and the corresponding energies with the V^{N-1} potential. This led to a correction of 5% for the ECP diagrams.

If j is a particle state excited from a hole state n, we put the restriction $m\neq n$ in the first summation in (16), and we get

$$\langle j3s|v|j3s\rangle - \langle j3s|v|3sj\rangle - \langle jn|v|jn\rangle + \langle jn|v|nj\rangle \quad .$$

This leads to the hole-particle ladder correction. If j state is in the continuum, the exact expression for the shifted energy denominator cannot be obtained. But the ladder diagrams with various numbers of horizontal interaction lines attached to particle lines gave contributions which fitted closely to a geometric series. By this process, a correction of 25% was obtained. The contributions from the ECP diagrams, both with and without ladder correction, are summarized in Table I, where k refers to continuum states and n refers to bound excited states. It is noted that the $1s$ and $2s$ contributions are of the same sign, in contrast to nitrogen and phosphorus atoms[6,7] where the unpaired electrons were in a p shell. In Table II, we present a breakdown of $2s\rightarrow ns$ contributions from the ECP diagrams for various excited (bound) ns states. It is noted that most of the bound-state contributions to ECP came from excitations to the lowest-lying $4s$ state, but the net contribution from

TABLE I. Core-polarization contribution to the hfs constant of sodium atom.

Diagram	Excitation	Contribution [a] (Mc/sec)
2(b)	$1s\rightarrow ns$ [a]	0.03946
	$1s\rightarrow ks$ [a]	28.03738
	Total	28.07684
		28.19273 [b]
		30.25803 [c]
	$2s\rightarrow ns$ [a]	1.79236
	$2s\rightarrow ks$ [a]	75.31573
	Total	77.10809
		81.12545 [b]
		104.97445 [c]
2(c)	$1s^-\rightarrow 3s^-$	0.06602
	$2s^-\rightarrow 3s^-$	4.36801
	Total	4.43403
	Grand Total	139.66651

[a] ns denotes excited bound s states and ks denotes continuum s states.

[b] Hole-hole ladder correction included.

[c] Hole-particle ladder correction included.

TABLE II. Contribution to core-polarization from $2s \rightarrow ns$ excitations.

Excitation	Contribution (Mc/sec)
$2s \rightarrow 4s$	0.99664
$2s \rightarrow 5s$	0.37866
$2s \rightarrow 6s$	0.18289
$2s \rightarrow 7s$	0.10203
$2s \rightarrow 8s$	0.06261
$2s \rightarrow 9s$	0.04109
$2s \rightarrow 10s$	0.02843
Total	1.79235

all the bound excited states is seen to be a small fraction of the total ECP result, indicating that the dominant contribution arose from the continuum excited states. In carrying out the required integration in k space in Eq. (15), we have used the Gauss-Laguerre quadrature procedure.[21] To apply this procedure most effectively, a test of the convergence of the continuum-state contributions was carried out as a function of k. Thus, Fig. 3 shows the plot of the integrand in Eq. (15) multiplied by the conversion factor C for $2s \rightarrow ks$ excitation as a function of k. It is observed that this curve has a peak around $k = 2.76$ a.u. and that, beyond this, the integrand decreases and is negligible beyond $k = 15$ a.u. A 12-point Gauss-Laguerre integration formula scaled to $k_{max} = 15$ a.u. was thus felt to be adequate for purposes of numerical accuracy.

Figures 2(d)–2(j) represent some of the important (1,1) diagrams. Thus, 2(d) and 2(e) represent modifications to the core-polarization diagram 2(b) resulting from a v interaction. Figures 2(f)–2(i) represent pure correlation effects which are absent in conventional Hartree-Fock theory.[10] Figure 2(f) with $a = 2p$ is associated with the correlation between $2p$ and $3s$ electrons while Fig. 2(g) is the corresponding residue diagram. Figure 2(h) with $b = 2p$ is the exchange counterpart of Fig. 2(g). Figure 2(f) also has an exchange counterpart which made negligible contribution. Figure 2(i) is similar to Fig. 2(f) except that it has the hfs vertex attached to the hole line. In addition to these diagrams, there were 159 other (1,1) diagrams. All of them have been calculated, and their total contribution, which was a small fraction of that from the important diagrams 2(d)–2(j), is included in Table III. A notable feature in Table III is that there is a great deal of numerical cancellation among the (1,1) diagrams in contrast to the lithium atom.[3] This cancellation is related to the presence of $2p$ core states in sodium. The total (1,1) contribution is found to be only 8.2 Mc/sec.

In Fig. 4, we present some important (0,2) diagrams. Only those diagrams which contribute more than 2 Mc/sec have been shown. The largest of these diagrams, namely 4(a)–4(d), are associated with a very important physical effect. This effect may be described as the alteration in the average spin-density produced at the nucleus by the $3s$ electron as a consequence of the mutual dynamic polarization it undergoes by correlation with core electrons. A (0,2) diagram describing a similar effect has also produced the most important correlation contribution in the lithium atom. Of these diagrams, the leading contribution arose from 4(a) and 4(b), which represent the influence of mutual polarization of the $3s$ valence electron

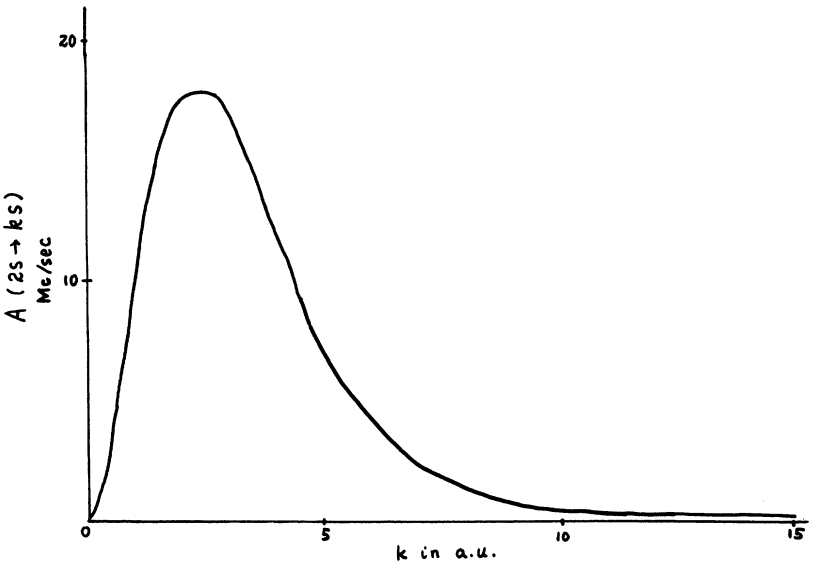

FIG. 3. Plot of the core-polarization contribution $A(2s \rightarrow ks)$ from $2s$ to continuum s-state excitation as a function of momentum k in atomic units.

TABLE III. Contributions from (1, 1) diagrams shown in Fig. 2.

Diagram	Description	Contribution (Mc/sec)
2(d)	$a=2s$, $b=1s$	1.45721
2(e)	$a=2s^{+}$, $b=2s^{-}$	1.37765
2(f)	$a=2s$	1.04259
	$a=2p$	8.64562
2(g)	$a=2s$	−7.20159
2(h)	$a=2p$, $b=2s$	1.11528
	$a=2s$, $b=2p$	1.18855
2(i)	$a=2s$, $b=2s$	5.36484
2(j)	$a=2s$	−5.02478
	Total	7.96537
	From other (1, 1) diagrams	0.24462
	Grand Total	8.20999

and $2p$ cores. The contributions from various orders of multipole in this mutual dynamic polarization are summarized in Table IV. The leading multipole polarization is seen to be the dipolar one described by the excitations ($3s \to kp$, $2p \to kd$) and ($3s \to kp$, $2p \to ks$) with the former being the dominant one. The monopole excitation ($3s \to ks$, $2p \to kp$) also makes sizeable contribution although somewhat less than the dipolar one. Quadrupolar excitations are seen to be relatively small in effect, and the higher-order multipoles gave virtually negligible contributions. Diagrams 4(c) and 4(d) represent similar polarization effects as in 4(a) and 4(b) with the s cores replacing the p cores. A similar breakdown of contributions from various orders of multipole excitations, as in the case of the p cores, is presented in Table V. Again, dipolar and monopolar excitations were found to be the most dominant with the former somewhat larger in effect. This feature is similar to that found for lithium. The diagrams involving $1s$ cores made negligible contributions. The net result from

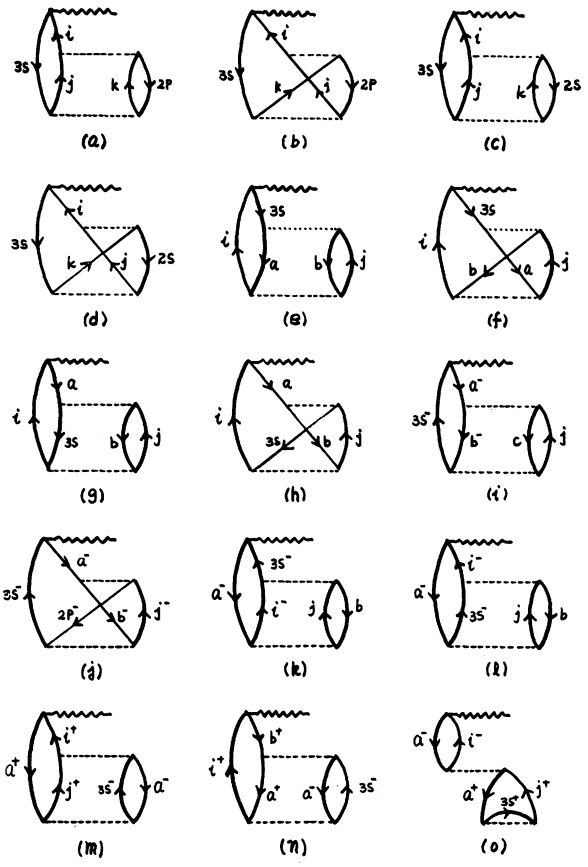

FIG. 4. Important (0, 2) diagrams.

diagrams 4(c) and 4(d) is seen from Table V to be about a factor of 5 smaller than that from 4(a) and 4(b) involving the $2p$ states. Figures 4(e)–4(h) are analogous to Figs. 4(a)–4(d) except that the second v vertex is attached to the hole lines instead of the particle lines. Figures 4(i)–4(n) are residue diagrams which occur because the electrons in core

TABLE IV. Contributions to the hfs constant from diagrams 4(a) and 4(b).

Intermediate angular momentum state [a]		Diagram 4(a)	Diagram 4(b)	Net contribution (Mc/sec)
j state	k state			
s	p	35.89074	−0.17579	35.71495
p	d	59.45898	−7.53940	51.91958
d	f	10.90661	−2.61233	8.29428
p	s	2.08103	−0.03756	2.04347
d	p	4.64963	−5.52615	−0.87652
f	d	3.66156	−2.52757	1.13390
			Grand Total	98.22966

[a] Includes contributions from both bound and continuum excited states.

TABLE V. Contributions to the hfs constant from diagrams 4(c) and 4(d).

Intermediate angular momentum state [a]	Diagram 4(c)	Diagram 4(d)	Net contribution (Mc/sec)
s	7.06577	−3.29113	3.77444
p	13.06313	−3.28161	9.7852
d	2.76235	0.19585	2.95817
f	1.52594	−0.61483	0.91111
		Total	17.42524

[a]Intermediate angular momentum states for 4(c) and 4(d) must be the same because the hole states involved are s states.

s^- states, while in the process of polarization, can get excited into the empty $3s^-$ state, whereas the core s^+ electrons are prohibited from doing this because the $3s^+$ state is occupied. Figure 4(o) describes the interplay between ECP and self-consistency effects. Thus, the ECP effect due to the $3s^+$ electron changes the wave function of the $1s^+(2s^+)$ state, which, through its self-consistent interaction with the $1s^-(2s^-)$ state, changes the density of the latter at the nucleus. In Table VI, we tabulate the contributions from diagrams 4(e) − 4(o) which add up to − 25.48 Mc/sec. In addition to these diagrams, there were 194 other (0, 2) diagrams whose total contribution added to only − 2.89 Mc/sec. A useful fact emerges from Table VI, which should simplify calculations in heavier atoms. The major contribution to these diagrams arises from $2s$-$2p$ and $2s$-$2s$ interactions, the effect of $2s$-$1s$, $2p$-$1s$, and $1s$-$1s$ being negligible. This is a result of the fact that all these diagrams also involve the valence state $3s$ which interacts most strongly with $2s$ and $2p$. Thus, in heavier alkali atoms (valence state ns), we expect the major contribution in these diagrams to come from $(n-1)s$ and $(n-1)p$ interactions. It is interesting also that while $2s$-$2s$ and $2s$-$2p$ contributions are individually comparable, the net $2s$-$2p$ contribution dominates because of the larger number of $2p$ states available.

In Fig. 5, we show some of the typical higher-order diagrams which were calculated to check the convergence of the BG perturbation procedure. Although there are numerous higher-order diagrams, their net effect is expected to be small because they are individually small and subject to substantial cancellations. In order to test this conjecture, we calculated diagrams 5(a)–5(g). Diagrams 5(a)–5(c) were selected because their par-

TABLE VI. Contributions from (0, 2) diagrams shown in Figs. 4(e)–4(o).

Diagram	Description	Contribution (Mc/sec)
4(e)	$a=2s^+,\ b=2s^-$	−2.81826
	$a=2s^+,\ b=2p$	−24.96961
	$a=2p,\ b=2s$	−3.11612
	$a=2p^+,\ b=2p^-$	−2.30202
4(f)	$a=2p,\ b=2s$	3.97638
	$a=2s,\ b=2p$	4.22965
4(g)	$a=2s,\ b=2s$	−2.17749
	$a=2s,\ b=2p$	−11.10126
4(i)	$a=2s,\ b=2s,\ c=2s^+$	2.63397
	$a=2s,\ b=2s,\ c=2p$	26.87874
4(j)	$a=2s,\ b=2s$	−4.50698
4(k)	$a=2s,\ b=2p$	−11.61920
4(l)	$a=2s,\ b=2p$	−12.65756
4(m)	$a=2s$	2.23073
4(n)	$a=2s,\ b=2s$	−1.79898
4(o)	$a=2s$	2.55349
	Total	−25.47831
	From other (0, 2)	−2.89659
	Grand Total	−28.37490

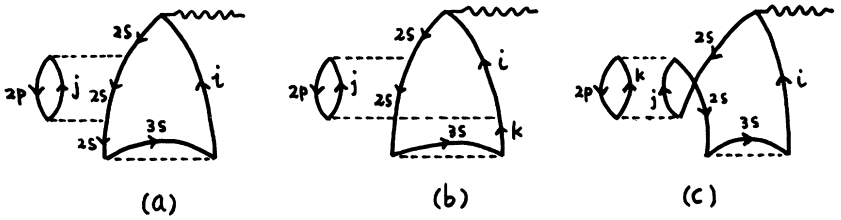

FIG. 5. Some higher-order diagrams.

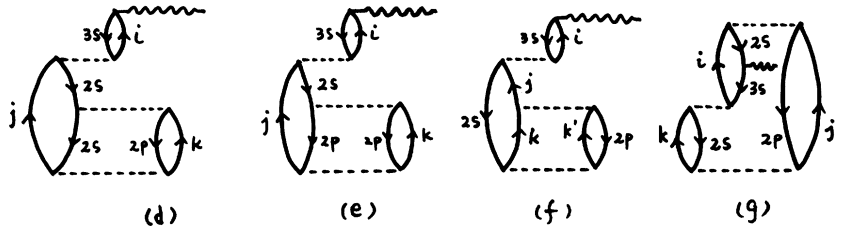

ent diagram (without the interaction on the 2*s* hole line) was 2(b), which was the largest of the diagrams shown in Figs. (2)–(4). From Table VII, diagram 5(a) is seen to contribute only 1.86 Mc/sec, which is about a factor of 40 smaller than diagram 2(b). Diagram 5(b) contributes −1.044 and thereby cancels a substantial part of the contribution from diagram 5(a). A similar cancellation was found among the remaining diagrams in Fig. 5. Figure 5(c) is a typical "rearrangement diagram"[5] whose contribution was found to be rather small.

Diagrams 5(d)–5(f) were selected because they represent modifications to the important polarization diagrams, Figs. 4(a)–4(d). They also include a limb involving 2*s*-2*p* correlation which was found important among some of the (0, 2) diagrams in Fig. 4. They are individually small and also substantially, cancel leading to a net result of only 0.25 Mc/sec, a negligible fraction of the contribution from parent diagrams 4(a)–4(d). Figure 5(g) is a typical three-particle diagram and, as in our earlier calculation,[6] its effect was found to be negligible. The net contribution from all these higher-order diagrams 5(a)–5(g) is seen to be only 0.238 Mc/sec. From our analysis of these diagrams, we do not expect that inclusion of additional higher-order diagrams will increase this small result dramatically.

The total contributions from (0, 0), (0, 1), (1, 1), and (0, 2) diagrams and their sums are listed in Table VIII and compared with experiment. Our final result is 857.8001 Mc/sec. We did not include the contributions from the higher-order diagrams in Fig. 5, since they were found to be small. An estimate of the probable error in our result due to this and other sources will be made in Sec.

TABLE VII. Contributions from some higher-order diagrams shown in Fig. 5.

Diagram	Contribution (Mc/sec)
5(a)	1.8572
5(b)	−1.0445
5(c)	−0.3256
5(d)	0.7390
5(e)	0.5286
5(f)	−1.5167
5(g)	0.0003
Total	0.2383

TABLE VIII. Net contribution from (0, 0), (0, 1), (1, 1), and (0, 2) diagrams.

Class of diagrams		Contribution [a] (Mc/sec)
(0, 0)		622.64360
(0, 1)		139.66651
(1, 1)		8.20999
(0, 2)		87.28000 [b]
	Total	857.80010
	Experiment	885.8131 ± 0.0001 [c]

[a] Does not include the contribution from Table VII.
[b] Includes the contributions from Tables IV, V, and VI.
[c] See Ref. 12.

IV, where we will compare our calculated result with earlier investigations and experiment.

IV. DISCUSSION

In this section, we shall first try to draw some inferences from the individual contributions in Tables I–VII concerning the importance of various physical effects that can contribute to the hfs of sodium. Subsequently, we shall consider the relationship between our results and experiment for the hfs constant, and comment on earlier theoretical results.

It appears from the results presented in Secs. I–III that the hfs for the sodium atom arises from three main sources: the direct contribution of the $3s$ orbital, exchange core-polarization, and intershell correlation. The direct contribution of 622.6436 Mc/sec is necessarily the same as from the RHF method. This is 70% of the experimental value of 885.8131 Mc/sec. The spin polarization [(0, 1) diagrams] contributes about 53% of the difference between the experimental and RHF values. The intershell-correlation effect contributes another 36%, thus bringing our result to within 97% of experiment. The (1, 1) diagrams in Fig. 2 contribute only 1% of experiment and about 9% of the total correlation contribution, the remainder of the latter originating from the (0, 2) diagrams. The importance of the (1, 1) diagrams has been related in the past[3] to the importance of having the total wave function as an eigenfunction of $\vec{S}^2$. The small magnitude of the (1, 1) contribution indicates that, as in the lithium atom, this eigenfunction behavior with respect to $\vec{S}^2$ is not an important consideration for hyperfine effects.

Our total result from all the diagrams is seen from Table IX to be in much better agreement with experiment than earlier values. We shall comment on these earlier results presently, but want to concentrate for the present on our result and experiment. The error estimate quoted for our result was arrived at from a consideration of various additional sources of contribution that could be important. One source of error is the neglect of higher-order diagrams beyond (0, 2). As we have already mentioned in Sec. III, we have examined various typical higher-order diagrams shown in Fig. 5 and found their contribution to be very small individually. In addition to this, there is a great deal of numerical cancellation among such diagrams, as may be seen from Table VII, and we do not anticipate that any other higher-order diagrams will be of larger order of magnitude than the typical ones shown in Fig. 5. From these considerations, we feel that ±3 Mc/sec is a conservative estimate of the error in the hfs constant due to neglect of higher-order diagrams. A second possible source of error is our neglect of hole-particle and particle-particle ladders beyond the (0, 1) diagrams. A conservative estimate of the error due to this source is about 3% of the total contribution from all the (1, 1) and (0, 2) diagrams, that is ±3 Mc/sec. The combination of these two error estimates leads to the quoted error range of ±6 Mc/sec for our result.

TABLE IX. Comparison of present result with earlier work and experiment.

Method	hfs constant A (Mc/sec)
Experiment [a]	885.8131 ± 0.0001
Semiempirical [b]	808
UHF (Numerical) [c]	764
(Analytical) [d]	772
MP [e]	771.54
Present Calculation	857.8001 ± 6

[a] See Ref. 12.
[b] See Ref. 22
[c] See Ref. 13.
[d] See Ref. 23.
[e] See Ref. 14.

In looking for reasons for the remaining small discrepancy between the results of our many-body calculation and experiment, we note that no account of relativistic effect has been made in our analysis. A recent Hartree-Fock–Dirac calculation[14] indicates that the direct contribution from $3s$ orbital should be increased by 13 Mc/sec (2% of the RHF) to include relativistic effects. In addition to this correction to the (0, 0) diagram, we have scaled all diagrams involving a hfs vertex associated with the $3s$ state by the ratio of the relativistic and nonrelativistic hyperfine amplitudes for the $3s$ state (≈ 1.01). This correction provides an additional 2 Mc/sec, leading to an estimated relativistic correction of 15 Mc/sec, and increasing our final result to 872.8 ± 6 Mc/sec. In addition to these relativistic corrections, there can be additional ones associated with the hyperfine vertices linked to $1s$ and $2s$ and excited s states, as well as from relativistic effects associated with other vertices. We expect the latter to be minimal in effect for a light metal like sodium. A complete understanding of relativistic effects will require a relativistic Brueckner-Goldstone (BG-Dirac) theory. It seems to us that a combination of the remaining relativistic effects or additional corrections due to radiative effects, finite nuclear structure, and Breit interaction can explain the small remaining discrepancy with experiment.

We would like next to comment on some of the other theoretical results listed in Table IX. The result obtained by Kjeldaas and Kohn[22] was based

on wave functions calculated in an empirical potential for the atom. In view of the empirical nature of the potential, they include indirectly some amount of correlation in their wave function, which accounts for the fact that their result is intermediate between our many-body result and one-electron UHF results. The first of the latter type of results in Table IX was obtained by Goodings[13] through numerical solutions of the self-consistent UHF equation. The second one was obtained from an analytic wave function obtained by Nesbet[23] using a variational procedure. The UHF procedure is an attempt to include the effects of ECP and hence should give a result comparable in principle to that from our (0,1) diagrams. However, the UHF wave function is known to suffer from the difficulty of not being an eigenfunction of $\tilde{S}^2$. It has been remarked earlier that (1,1) diagrams, which in the present case are only 1% of our final result, are a measure of the importance of the $\tilde{S}^2$ eigenfunction behavior of the wave function. This observation, combined with the fact that in alkali atoms, unlike the situation in incomplete p-shell atoms,[5-7] no large cancellations between ECP contributions from individual core states are involved, explains the good agreement between the ECP result from the UHF procedures and our (0,1) contribution.

The MP result[14] listed in the fourth row of Table IX compares well with our (0,1) contribution, as was also found to be the case for other atoms. This is expected, since MP procedure is also a perturbation approach involving small numbers and is also not susceptible to serious errors encountered with the $\tilde{S}^2$ eigenfunction nature of the wave function. We do note, however, that the MP result (141.54 Mc/sec) is a little larger than the BG result (135.23 Mc/sec) from diagram 2(b). It is observed that the MP contribution should be compared with the contribution from diagram 2(b) alone, since effects like that represented by diagram 2(c) are not included in the MP approach. This feature, that the MP procedure gives a larger value than the diagram 2(b) of BG theory, seems to persist in a number of instances where results by both approaches are available.[3,6-8] We conjecture that this is a result of the local approximation[24] used in the MP procedure.

The BG procedure has been shown to provide an understanding of the contributions to the hfs constant of sodium atom from various physical interactions in the atom. The calculated correlation contribution was found to be sufficient to bridge the gap between one-electron theory and experiment.

In the present instance (and various earlier cases where BG calculations are available) the diagrams up to and including second-order and associated ladders are found to be sufficient to explain observed hfs constant. Since these diagrams include essentially all two-particle correlations, correlations involving larger number of particles are expected to have minimal effect in atoms. Such an observation has also been made from investigations of correlation energy.[25]

ACKNOWLEDGMENT

The authors gratefully acknowledge the help rendered by the staff of the computing center at the University of California, Riverside, California.

---

*Present address: Department of Physics, University of Utah, Salt Lake City, Utah 84112.

†Supported by the National Science Foundation.

[1]J. Goldstone, Proc. Roy. Soc. (London) A239, 267 (1957); K. A. Brueckner, Phys. Rev. 97, 1353 (1955); 100, 36 (1955); The Many-Body Problem (John Wiley & Sons, Inc., New York, 1959); T. D. Schultz, Quantum Field Theory and the Many-Body Problem (Gordon and Breach, Science Publishers, Inc., New York), Chap. III.

[2]H. P. Kelly, in Perturbation Theory and its Application in Quantum Mechanics, edited by C. H. Wilcox (John Wiley & Sons, Inc., New York, 1966), p. 215.

[3]E. S. Chang, T. P. Das, and R. T. Pu, Bull. Am. Phys. Soc. 12, 69 (1967); E. S. Chang, R. T. Tu, and T. P. Das, Phys. Rev. 174, 1 (1968).

[4]C. Matsubara, N. C. Dutta, Robert T. Pu, and T. P. Das, Phys. Rev. 177, 33 (1968).

[5]H. P. Kelly, Phys. Rev. 173, 142 (1968).

[6]N. C. Dutta, C. Matsubara, R. T. Pu, and T. P. Das, Phys. Rev. 177, 33 (1968).

[7]N. C. Dutta, C. Matsubara, R. T. Pu, and T. P. Das, Phys. Rev. Letters 21, 1139 (1968).

[8]J. D. Lyons, R. T. Pu, and T. P. Das, Phys. Rev. 178, 103 (1969).

[9]H. P. Kelly, Phys. Rev. 180, 55 (1969).

[10]R. E. Watson and A. J. Freeman, Hyperfine Interactions (Academic Press Inc., New York, 1967), p. 53.

[11]N. Bessis, H. Lefebvre-Brion, C. M. Moser, A. J. Freeman, R. K. Nesbet, and R. E. Watson, Phys. Rev. 135, A588 (1964).

[12]M. Arditi and R. T. Carver, Phys. Rev. 109, 1012 (1958); P. Kusch and H. Taub, *ibid.* 75, 1477 (1949).

[13]D. A. Goodings, Phys. Rev. 123, 1706 (1961).

[14]L. Tterlikkis, S. D. Mahanti, and T. P. Das, Phys. Rev. 176, 10 (1968).

[15]See, Silvan S. Schweber, An Introduction to Quantum Field Theory (Harper & Row Publishers, Inc., New York, 1962), Chaps. 6 and 11.

[16]A. Burgess, Proc. Phys. Soc. (London) 442, 81 (1963).

[17]E. Clementi, IBM J. Res. Develop. 9, 2 (1965).

[18]E. Fermi, Z. Physik 60, 320 (1930).

[19]The values of the constants are taken from the following sources: $\mu_N(Na^{23})$, H. F. Ramsey, Nuclear Moments, (John Wiley & Sons, Inc., New York, 1953); μ_B, a_B, and $\hbar$, R. B. Leighton, Principles of Modern Physics (McGraw-Hill Book Co., Inc., New York, 1959).
[20]Superscript ± will henceforth be used to denote one-electron spin states, both in the text and in the diagrams.
[21]Z. Kopal, Numerical Analysis (John Wiley & Sons, Inc., New York, 1961).
[22]T. Kjeldaas and W. Kohn, Phys. Rev. 101, 66 (1956).
[23]R. K. Nesbet, Quantum Theory of Atoms, Molecules and the Solid State, edited by P. O. Löwdin (Academic Press Inc., New York, 1966).
[24]G. D. Gaspari, W. M. Shyu, and T. P. Das, Phys. Rev. 134, A852 (1964).
[25]E. U. Condon, Rev. Mod. Phys. 40, 872 (1968).

PHYSICAL REVIEW A VOLUME 1, NUMBER 4 APRIL 1970

Electric Field Effect in the Resonance Lines of Indium and Thallium†

Thomas Richard Fowler* and Joseph Yellin
Lawrence Radiation Laboratory, University of California, Berkeley, California 94720
(Received 3 November 1969)

The atomic-beam method has been used to study the Stark effect in the resonance lines of indium ($6s\,^2S_{1/2} \rightarrow 5p\,^2P_{1/2}$, 4102 Å) and thallium ($7s\,^2S_{1/2} \rightarrow 6p\,^2P_{1/2}$, 3776 Å). The difference between the atomic polarizability of the $^2S_{1/2}$ state and that of the $^2P_{1/2}$ state [$\Delta\alpha(sp)$] has been determined and compared with calculations in the Coulomb approximation. For indium, we find $\Delta\alpha(sp) = 138(11) \times 10^{-24}$ cm^3 and for thallium $\Delta\alpha(sp) = 115(12) \times 10^{-24}$ cm^3.

I. INTRODUCTION

Although the perturbation of atomic levels by electric fields was first observed more than forty years ago,[1] there has been little progress by way of a systematic study of the Stark effect on free atoms until the present decade. This has been due to the experimental difficulties of measuring small frequency shifts and attaining high electric fields, as well as theoretical difficulties in calculating and interpreting experimental results. Unlike the Zeeman effect, which depends only on the angular part of the wave function and can be calculated accurately for any atomic state, the calculation of the Stark effect involves infinite sums of radial integrals requiring accurate radial wave functions for excited states.

Recently, there has been a resurgence of interest in the electric field effect. The renewed activity is due to the successful application of new experimental techniques to the Stark effect and to theoretical developments. In addition, interest has been generated by the application of the Stark effect to the search for electric dipole moments in elementary particles,[2–4] and the measurement of isotope shifts[5] and hyperfine structure of excited states.[6,7] On the experimental side, atomic-beam[8] level-crossing,[9,10] and optical double-resonance[11] techniques have been used to observe differential Stark shifts between levels of an atomic state as well as shifts between levels belonging to two different states (optical Stark shift).[12] To observe the differential shifts within a state $\approx 10^{-8}$ to 10^{-6} Hz/(kV cm^{-1})^2, relatively low electric fields (< 100 kV/cm) are required on account of the precision attainable in radiofrequency spectroscopy. To observe and measure the Stark shift in optical transitions requires large electric fields (> 100 kV/cm), which are required because of the linewidths associated with optical transitions and the calibration procedure, which involves large Stark shifts of approximately 10^3 MHz. Thus techniques had to be developed for achieving high electric fields. On the theoretical side, methods have been developed for treating the infinite sums appearing in the Stark effect[13,14] and calculating the radial integrals needed.[15]

In the present experiment, the atomic-beam method was used to investigate the Stark shift in the 4102 Å line of indium and the 3776 Å line of thallium. This experiment serves as an important preliminary to the measurement of isotope shifts in indium by the atomic-beam method.

II. EXPERIMENTAL METHOD

The experimental method employed here has been described previously in connection with the Stark-shift measurements in the D_1 lines of cesium, rubidium, and potassium.[12,16] The application of the